Materials Transactions, Vol. 49, No. 4 (2008) pp. 746 to 753

Fusion Zone Microstructure Evolution of Al-Alloyed TRIP Steel in Diode Laser Welding

Mingsheng Xia[1,2], Zhiling Tian[2], Lin Zhao[2] and Y. Norman. Zhou[1]

[1]*Centre for Advanced Materials Joining, University of Waterloo, Waterloo, Ontario, Canada*
[2]*State Key Laboratory of Advanced Steel Processes and Products, Central Iron & Steel Research Institute, Beijing, P. R. China*

TRansformation Induced Plasticity (TRIP) steels are promising materials to achieve a better combination of formability and strength than conventional steels due to their unique microstructural makeup. Though welding is a vital part of auto body manufacturing, the weldability of TRIP steels has some complex and poorly understood features, which has served to retard the growth of its applications in the automotive industry. In this study, autogeneous welds were carried out on Al-alloyed TRIP steel using a 4 kW diode laser. Both fusion zone solidification behavior and subsequent austenite transformation products were investigated with optical microscopy (OM), scanning electron microscopy (SEM) and transmission electron microscopy (TEM) techniques. In terms of solidification behavior, fusion zones solidified with high temperature δ-ferrite as the primary phase. Fusion zone microstructure at room temperature was composed of ferrite with a skeletal morphology characteristic of solidification, and austenite decomposition products almost all having a lath morphology. Skeletal ferrite covered about 30% fusion zone area. Upper bainite laths separated by retained austenite films comprised most of the transformed microstructure, about 65% of the fused area. Lower bainite with carbide particles dispersed in an aligned way, chunk shaped retained austenite, lath martensite and twinned martensite were also occasionally observed. The Al content was considered to be for a dominant influence on fusion zone microstructure evolution. [doi:10.2320/matertrans.MRA2007271]

(Received November 6, 2007; Accepted January 21, 2008; Published March 25, 2008)

Keywords: *fusion zone, microstructure evolution, transformation induced plasticity (TRIP) steel, diode laser welding*

1. Introduction

The use of high strength steels has increased in the automotive industry in order to reduce automotive body weight. In general, steels of increased strength have significantly reduced ductility and formability, and considerable research efforts have been carried out to develop steel grades with both a high strength and a high elongation. TRansformation Induced Plasticity (TRIP) steels are a promising solution to achieve a better combination of formability and strength than conventional steels.[1)] The microstructure of these steels typically consists of polygonal ferrite, bainite, martensite, and retained austenite (about 10–20%). The main phenomenon responsible for the improved mechanical properties has been proposed to be the deformation-induced transformation of the metastable retained austenite to martensite during straining.[1)]

The standard CMnSi TRIP steel contains typically about 0.15 mass % C, 1.0–2.5 mass % Si and 1.0–3.0 mass % Mn. Si is added to suppress cementite formation during the bainite holding temperature. However, the latter two elements form a very stable Mn_2SiO_4 oxide film on the surface during the annealing process. The surface tension properties of this oxide, when in contact with liquid Zn, inhibit the galvanisability[2)] and as a result the TRIP steels are currently generally electrogalvanised rather than hot dipped galvanized. Alternative alloy elements could be considered. Possible candidates to substitute for Si are Al, P and Cu which are known to play a somewhat similar role as Si.[3–7)] CMnAl TRIP steels have received much attention. Both Si and Al are insoluble in cementite and can greatly retard the cementite formation.[8)]

According to Meyer,[9)] the partial replacement of Si by Al in TRIP steels results in a much improved galvanisability. Maki[10)] also conducted research on the galvanisability of Si-free CMnAl and Al-free CMnSi TRIP steels respectively and similar results were obtained. Furthermore, the mechanical properties of cold rolled Si free CMnAl TRIP steel were comparable to those of conventional CMnSi TRIP steels.[11)] The Al-bearing TRIP steel exhibits a remarkable TRIP effect during tensile testing, comparable to Si-containing grades.[7)] The disadvantage of Al is its lower solid solution hardening capability than Si.[12)] As a result, the recent CMnSiAl TRIP steel is based on the concept of partial replacement of Si by a limited amount of Al.[13)]

In welding research area, some work has been conducted on the effects of laser welding processes on Si-alloyed TRIP steel.[14–16)] The fusion zone microstructure was revealed to be predominantly martensitic. But as for Al-alloyed TRIP steel welding, no systematic work in terms of fusion zone microstructure evolution has been reported up to now. In a previous paper, TEM and nanoindentation techniques were employed to characterize lathy phases mainly from the standpoint of crystallography.[17)] In this work, a comprehensive study on the fusion zone microstructure evolution (including solidification and solid-state transformation) of Al-TRIP steels with diode laser welding process is reported. The role of Al in fusion zone microstructure evolution has been evaluated as well.

2. Experimental Procedures

The steel used in this work had a chemical composition of Fe-1.5C-1.73Al-2Mn by weight, and was supplied as sheet of 1.2 mm thickness. It was designed to contain sufficient Al to prevent the cementite precipitation during holding at bainitic temperature range. About 2 mass % of Mn was added for the purpose of maintaining hardenability. The base metal microstructure, shown in Fig. 1, consisted of ferrite, bainite/

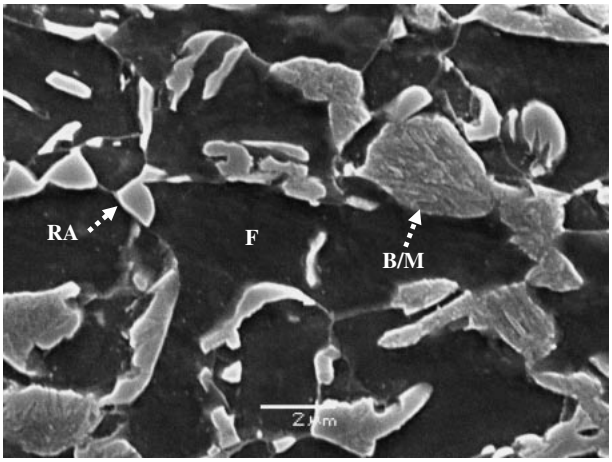

Fig. 1 SEM observation on base metal microstructure.

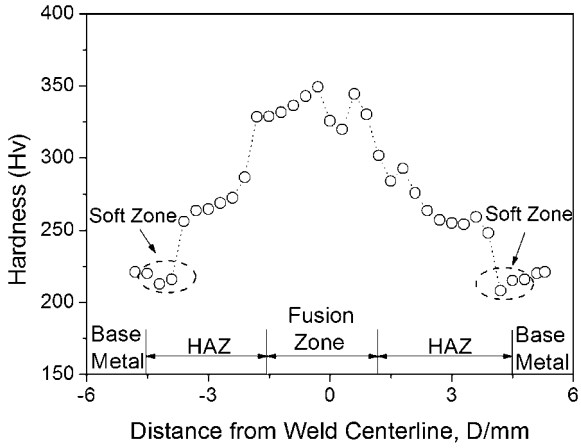

Fig. 2 Weld hardness profiles at the welding speed of 1.6 m/min (load: 500 g, loading time: 15 s).

Table 1 The characteristics of diode laser.

Laser machine	Laser type	Power (kW)	Focal length (mm)	Beam size (mm)	Wavelength (μm)
Nuvonyx ISL-4000L	Diode	4	80	0.9 × 12	0.8

martensite and retained austenite.

Experimental welds were carried out with the 4 kW diode laser under welding speeds ranging from 1.6 to 2.2 m/min. Full penetration was obtained in all welds. The details of the laser are shown in Table 1. Argon was employed as shielding gas from the top surface at the flow rate of 30 l/min. After welding, transverse samples were cut from representative welds for polishing, etching and metallographic observation. Vickers microhardness testing was conducted on nital etched samples. Fusion zone microstructure characterization was carried out by optical micrography (OM), scanning electron micrography (SEM) and transmission electron micrography (TEM) techniques.

3. Results

3.1 Hardness profiles and fusion zone microstructure overview

Figure 2 showed the typical weld hardness profiles with the welding speed of 1.6 m/min. The fusion zone microhardness was well above the base metal value and averaged 334 Hv. Outside of the fusion zone through the heat affected zone (HAZ), the hardness showed a decreasing trend. A soft zone was exhibited in the outer HAZ, which was beyond the scope of this paper. OM and SEM observations showed that the fusion zone was composed almost entirely of two kinds of constituents, ie, skeletal ferrite having a dendritic appearance (about 30% of the fusion zone area), and austenite decomposition products consisting of packets of laths, Fig. 3. The skeletal ferrite was believed to be beneficial to fusion zone ductility.[18] Higher magnification observation with SEM, Fig. 3(c), showed that the majority of the lathy products had the appearance of upper bainite and was about 65% of the fusion zone area.

Figure 4 showed the average fusion zone hardness (more than 5 indentations) under all welding speeds. With the increase of welding speed, fusion zone hardness showed only a slight increase. This confirmed that there was no significant microstructure difference among the welding speeds employed. As a result, welds made at the welding speed of 1.6 m/min were selected for further study.

3.2 Lathy microstructure

As shown in Fig. 5(a), most of the volume of transformation products comprised ferrite laths of a sideplate or upper bainite morphology in large groups of packets of parallel units with individual laths being separated by low angle boundaries. Fig. 5(b) was the higher magnification image of the rectangular area in Fig. 5(a). Bright field (BF) and dark field (DF) images revealed the presence of thin films sandwiched between laths. The selected area electron (SAE) diffraction pattern identified the film-like phase as retained austenite, Fig. 5(c).

Due to the fact that the morphology of upper bainite is similar to that of lath martensite because of the similarity of lattice parameters and crystal structure between them,[19] it is impossible to distinguish lath ferrite from lath martensite by SAE diffraction because conventional electron diffraction is not sensitive to small lattice parameter change between them. Vickers microhardness testing with the load of 50 g was employed to identify each other. The optical micrograph with hardness indentation and corresponding values was shown in Fig. 6. So it was expected fusion zone contained both upper bainite (308 Hv) and martensite (388 Hv) according to the literature in which upper bainite and martensite microhardness was 313 Hv and 428 Hv respectively.[20] Nanoindentation technique also revealed the presence of upper bainite and martensite from a nano-scale,[17] which agreed with the results in this work from a micro-scale.

Another lathy microstructure with different morphology was occasionally found under TEM observation, shown in Fig. 7. Inside the laths were aligned rows of precipitated carbide particles identified by their SAE diffraction patterns. This structural form is commonly referred to as lower bainite. Its crystallographic features are similar to those of upper

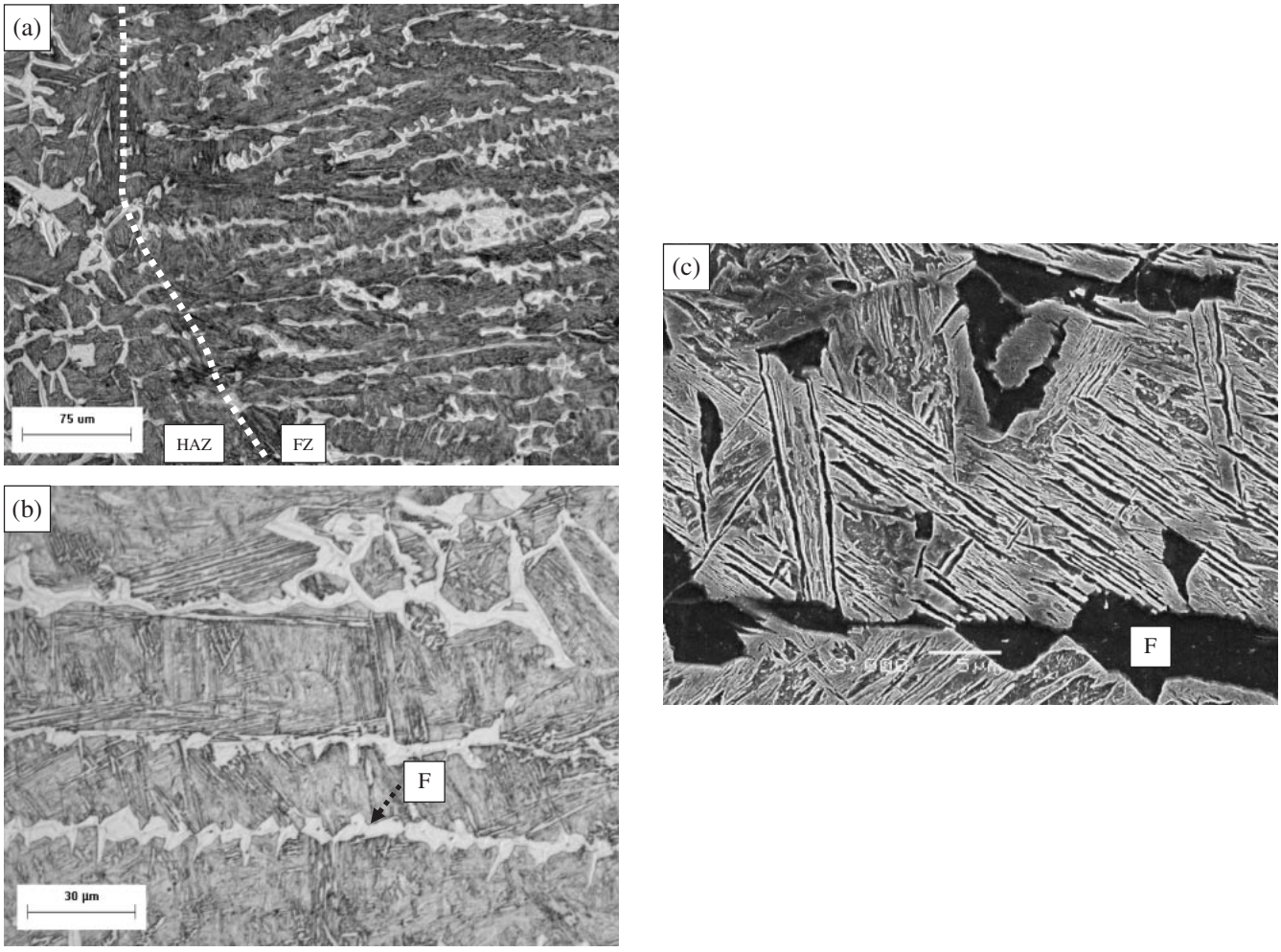

Fig. 3 (a) OM showing skeletal ferrite in fusion zone. Dotted line is the fusion zone boundary. (b) OM showing the fusion zone with higher magnification. (c) SEM observation on fusion zone.

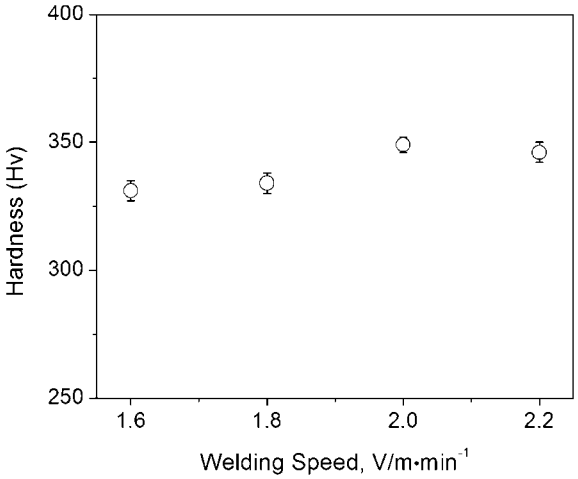

Fig. 4 Fusion zone hardness variation according to welding speed.

bainite except that cementite particles precipitate inside the laths of lower bainite.[8)]

3.3 Minor phases dispersed in the ferrite matrix

Apart from the film-like retained austenite between laths revealed above, some chunk-shaped austenite islands were observed. Figure 8(a) and (b) was the bright and dark image respectively with the SAD pattern of a typical particle of retained austenite. Similarly, twinned martensite as an island was also found in the fusion zone, Fig. 9. However, these two phases were not frequently observed.

4. Discussions

4.1 Solidification behavior

According to the results above, it was found that ferrite was one of the predominant phases in fusion zone, which rarely happened in the laser welding of automobile steel with such high carbon content. Compared to conventional high strength low alloy steel, the investigated steel contained high level of Al content to suppress cementite precipitation during bainitic holding temperature range. Different from typical composition alloyed with Si in TRIP steel, Al is a strong ferrite stabilizer and can promote the formation of ferrite in the fusion zone microstructure evolution through the following ways, which can be found in a quasi-binary phase diagram for a composition close to the steel being studied (Fe-Mn-Al-C), calculated with thermo-calc software,[21)] shown in Fig. 10. Firstly, Al helps the fusion zone solidify with δ-ferrite as primary phase, which has been confirmed in

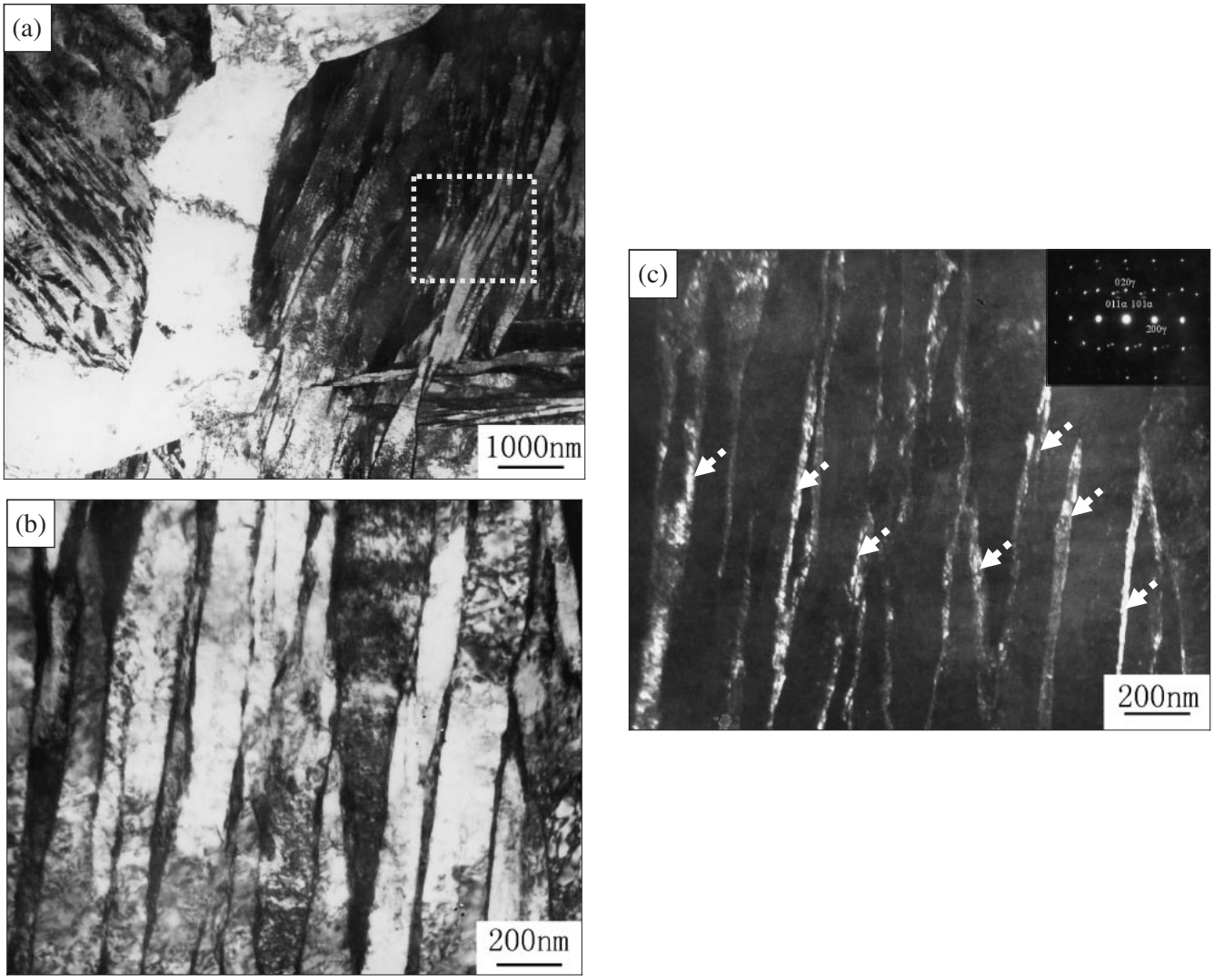

Fig. 5 Laths with retained austenite films: (a) Ferrite and lath phases; (b) BF image of rectangle area in (a); (c) DF image of rectangle area in (a).

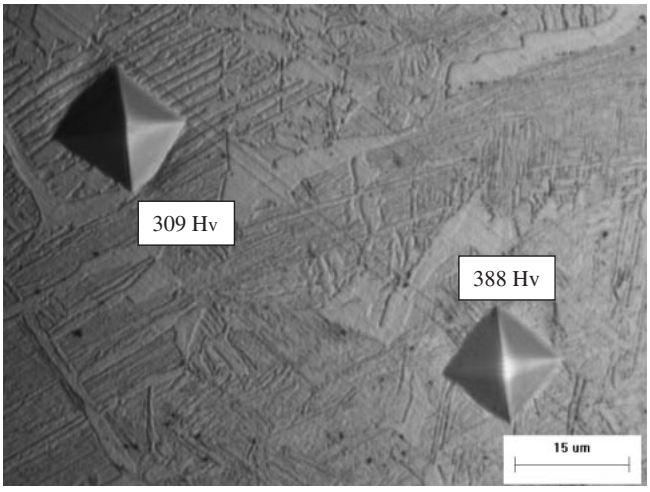

Fig. 6 Indentations with corresponding hardness values.

many cases even with the cooling rate as high as 10^3 K/s.[22] Secondly, Al can significantly shrink the austenite single phase region and markedly widen the two phase ($\delta + \gamma$) region. And furthermore, with the increase of Al content, the two-phase region shrinks gradually until the appearance of single ferrite phase region. Thirdly, in austenite decomposition process, Al-rich austenite can push the critical cooling rate to a high level for polygonal ferrite formation. According to the CCT diagram of the Al-alloyed TRIP steel obtained by earlier workers, the polygonal α-ferrite can form from austenite decomposition within a wide range of cooling rate, even up to 200 K/s,[23] higher than that of present work, ranging from 50 to 100 K/s depending on welding speed.

According to the calculated equilibrium phase diagram (Fig. 10), δ-ferrite should be the first solid to form, and in fact for the investigated steel chemistry, the liquid should be completely transformed to δ-ferrite before any austenite forms ($L \rightarrow \delta$). If that were to occur, the first austenite to form would be in the inter-dendritic regions during further cooling ($\delta \rightarrow \delta + \gamma$).

However, during rapid, non-equilibrium solidification of these welds, the solute segregation (primarily C and Mn) into the inter-dendritic liquid would eventually cause a shift from ferrite to austenite solidification, so that the last liquid to freeze, in between the δ-ferrite dendrites, was austenite.

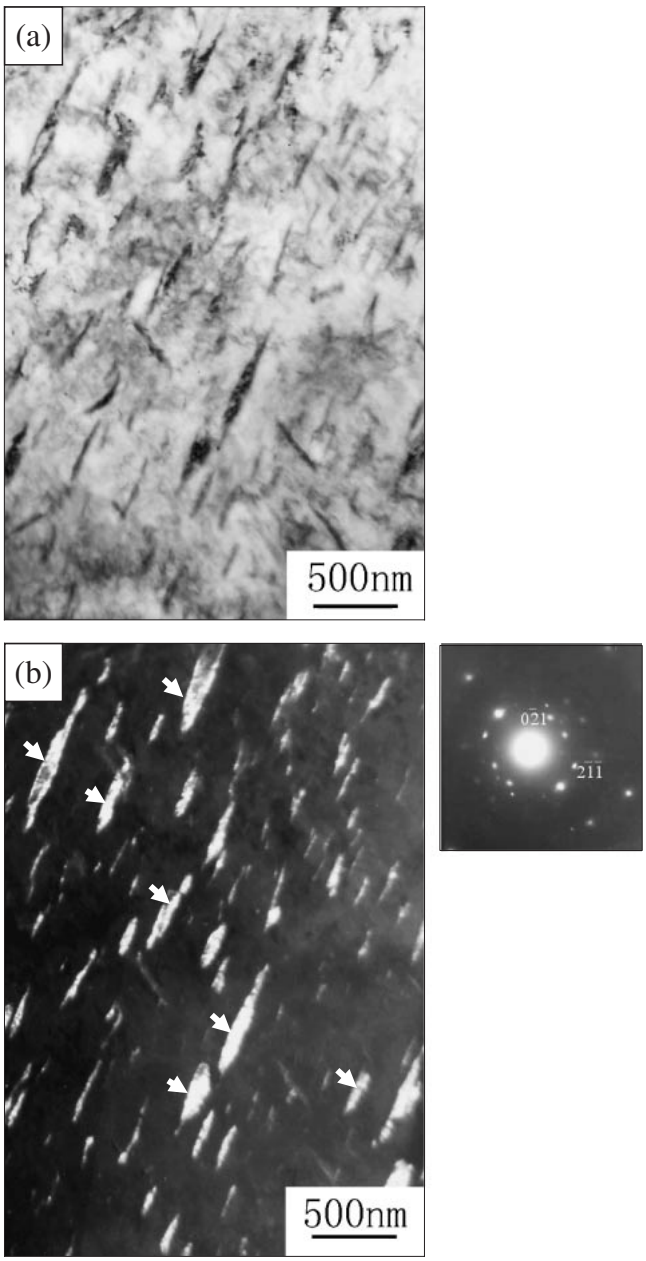

Fig. 7 Lower bainite: (a) BF image; (b) DF image.

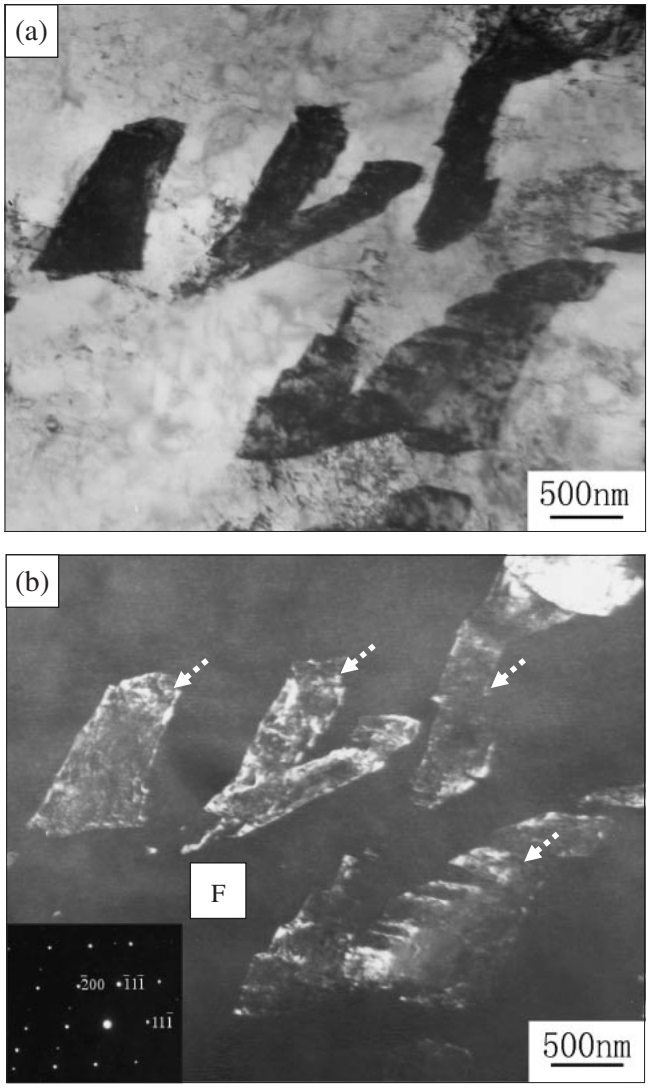

Fig. 8 Massive retained austenite: (a) BF image; (b) DF image.

The solidification sequence would become: L→δ+L and δ+L→δ+γ (with peritectic reaction), which is illustrated in Fig. 11. Fig. 11(a) and (b) showed that high temperature δ-ferrite solidified as the primary phase and grew into the liquid with dendritic morphology. With continued solidification, the local composition of the remaining interdendritic liquid moved to the left of the investigated steel chemistry represented by the dotted lines in Fig. 10, inducing a shift to austenite formation from the last remaining liquid. As a result, the austenite can form from the peritectic reaction between the remaining liquid and δ-ferrite.

In either case, the end result is the same, i.e., dendritic δ-ferrite and inter-dendritic austenite (Fig. 11(c)). With further cooling, austenite would decompose into other phases depending on cooling conditions. The room temperature microstructure was shown in Fig. 3(a) and it showed that the δ-ferrite retained a dendritic morphology, characteristic of solidification product. In summary, therefore, the pattern of ferrite in the fusion zone suggests that it solidified as primary ferrite dendrites which subsequently transformed incompletely to austenite during cooling leaving ferrite filaments along centers of the former dendrites in a manner similar to that previously described for stainless steels.[24)]

4.2 Austenite decomposition

The austenite in the intermediate temperature range would undergo transformation in the subsequent cooling process. Due to high content of Al, it was expected that the α-ferrite would nucleate epitaxially on the present high temperature δ-ferrite according to Al-alloyed TRIP steel CCT diagram,[23)] which frequently happened to dual phase steel in the similar way after cooling from intercritical phase region.[25)] Note that the δ and α-ferrites are identical in crystal structure which means no structure interface between the two types of ferrite and α-ferrite is an extension of δ-ferrite. The terminology does however help distinguish the δ-ferrite which formed as dendrites during the solidification of liquid and α-ferrite which occurred by solid state transformation of austenite.

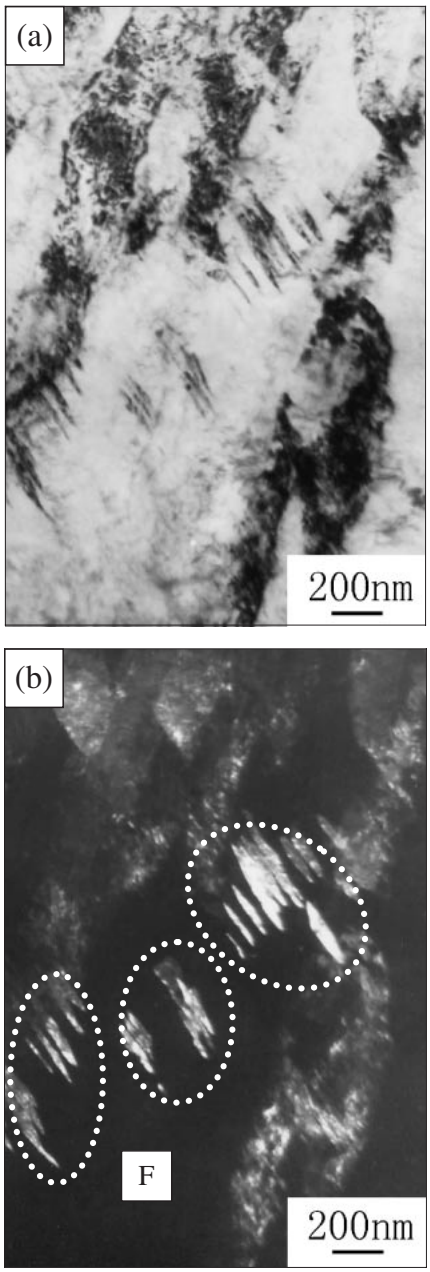

Fig. 9 Twinned martensite in dotted circles: (a) BF image; (b) DF image.

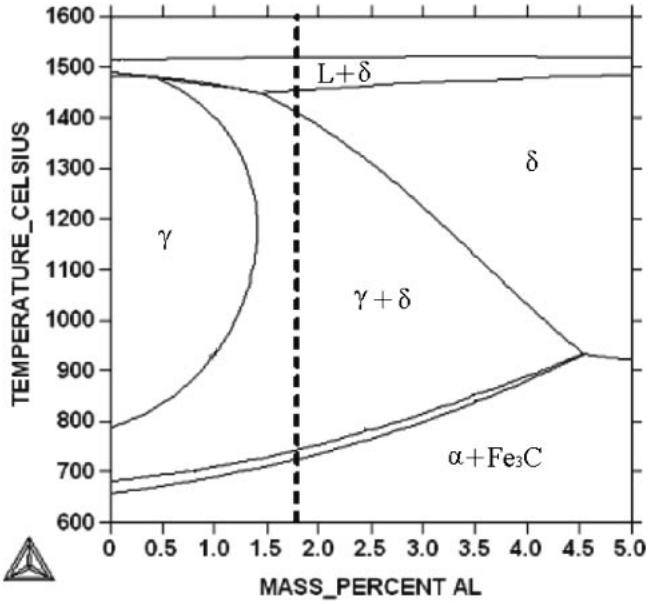

Fig. 10 Calculated quasi-binary phase diagram for a composition close to the steel being studied (Fe- Mn - Al -C)(Dotted line indicates the investigated steel chemistry).

Apart from ferrite, the rest of transformation products will be detailed separately as follows.

(1) Lathy Microstructure (Upper bainite, Lower Bainite and Martensite)

Upper bainite was another major constituent in fusion zone. The form of the product of a bainite transformation varied with transformation temperature or cooling conditions after welding and alloy composition. The upper bainite that formed at higher temperature comprised a series of parallel ferrite laths separated by semi-continuous retained austenite as discussed above. In the higher temperature range, carbon atoms were sufficiently mobile to either partition ahead of the austenite-ferrite interface, or to diffuse from the ferrite to the austenite immediately after ferrite formation. In either case, the carbon-enriched austenite was achieved. However, lower bainite formed at lower temperatures, and in this phase the ferrite contained an intra-ferritic distribution of carbide particles. The carbide particles in lower bainite shared a discrete orientation relationship with the ferrite, but almost invariably there was only one orientation of lenticular carbide particles within each ferrite crystal in this case probably due to the low carbon content or absence of externally applied stress.[26)]

As for cooling conditions in these diode laser welding experiments, the fusion zone cooling rate (50–100 K/s through the bainite transformation range) was low enough for formation of both kinds of bainites. In alloying aspects, Al accelerated the bainite formation[27)] and increased bainitic transformation kinetics due to higher nucleation rate promotion according to Mertens.[28)] In comparison, markedly different from the multiphase microstructure exhibited by the Al-alloyed TRIP steel fusion zone, Si-alloyed TRIP steel produced almost monophase, namely martensitic, fusion zone under the diode welding process.[18)] The difference in two TRIP steels was attributed to the alloying element choice of Al and Si, since the latter could significantly increase its hardenability and promote martensite formation.[23)]

(2) Minor Phases Dispersed in Ferrite Matrix

For the filmy retained austenite between sheaves of laths, it was mainly due to the chemical stabilization (C segregation) and mechanical stabilization arising from the volume expansion in martensite or bainitic transformation.[29)] In terms of the chunk-shaped islands dispersed in ferrite matrix, it means this austenite was the last part remaining during the high temperature austenite decomposition, and it evidently contained preferential enrichment of solutes, like carbon, increasing its hardenability and decreasing martensite transformation starting temperature (Ms). The presence of sufficient quantities of Al could efficiently retard the cementite formation due to its insolubility in cementite, which had the effect of making C more available to segregate into residual austenite. Mn as high as

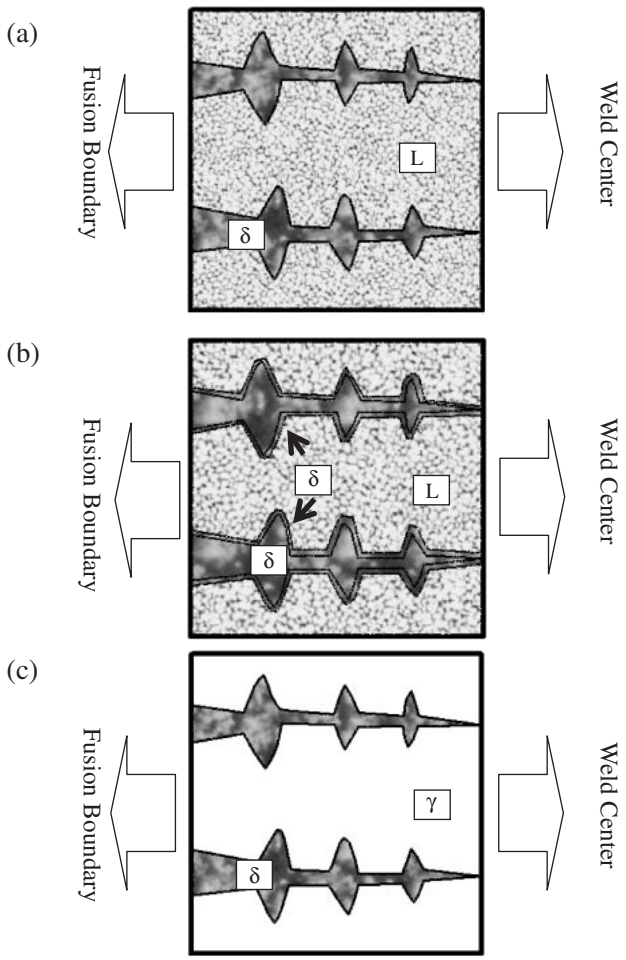

Fig. 11 Schematic graphs showing solidification in fusion zone.

2 mass % also contributed to austenite stability.[30] The formation of retained austenite manifested two points. Firstly, it was well known that diode laser welding process is one with intermediate cooling rate arising from its unique rectangular beam size, shown in Table. 1. The cooling rate was high enough to narrow the high temperature duration and the time for retained austenite decomposition. Secondly, the presence of retained austenite in fusion zone probably enables it have the TRIP effect, which is desired in TRIP steel welding in order to achieve matching properties with base metal. But it needs further investigation because there are many factors of retained austenite influencing the mechanical properties, like volume fraction, grain size and morphology.[31]

5. Conclusions

The response of Al-TRIP steel with diode laser welding process was investigated at welding speeds ranging from 1.6 to 2.2 m/min. The fusion zone microstructure evolution at the welding speed of 1.6 m/min was inferred based on microstructural observation at room temperature. The conclusions are summarized as follows.

(1) Fusion zone microstructure at room temperature was composed of ferrite, at about 30% of the fusion zone area with a skeletal morphology characteristic of solidification, and austenite decomposition products almost all having lath morphology.
(2) The skeletal morphology is believed to be caused by incomplete transformation of primary δ-ferrite to austenite leaving dendrtic δ-ferrite filament retained even down to room temperature. The subsequent austenite decomposition resulted in α-ferrite, formed on the existing δ-ferrite filament, and room temperature dendritic morphology.
(3) Other austenite decomposition products formed in welding included upper bainite (about 65% of the fusion area), martensite laths and retained austenite (interlath films as well as blocky), lower bainite and occasionally observed twinned martensite.
(4) Al was predominately responsible for this fusion zone microstructure evolution, skeletal ferrite plus mainly upper bainite, compared to mostly martensite in Si-alloyed TRIP steels.

Acknowledgement

This article was financially supported by Auto21 (www.auto21.ca), Dofasco, Huys Industries Ltd., Centerline Ltd., and ILZRO.

REFERENCES

1) V. F. Zackay, E. R. Parker and R. Busch: Trans. ASM. **60** (1967) 252–259.
2) M. Isobe, C. Kato and K. Mochizuki: Proc. 39th Conf. on Mechanical Working and Steel Processing, Indianapolis, IN, USA, October 1997, ISS, 121.
3) H. C. Chen, H. Era and M. Shimizu: Metall. Trans. A. **20** (1989) 437–441.
4) B. Liesbeth, V. Kim and E. Wettinck: ISIJ Int. **46** (2006) 1251–1257.
5) A. Pichler and P. Stiazny: Steel Res. **70** (1999) 459–465.
6) M. D. Meyer, D. Vanderschueren and B. C. De. Cooman: ISIJ Int. **39** (1999) 813–822.
7) E. Giraulta, A. Mertensb, P. Jacquesb, Y. Houbaertc, B. Verlindena and J. V. Humbeecka: Scr. Mater. **44** (2001) 885–891.
8) H. K. D. H. Bhaeshia and R.W.K. Honeycombe: *Steel microstructure and properties*, 3rd edition 2006, Published by Elsevier Ltd.
9) J. Mahieu, S. Claessens, M. D. Meyer and B. C. De. Cooman: *Proc. On Galvanised Steel Sheet Forum–Automotive*, (London, UK, May 2000, The Institute of Materials), pp: 185.
10) J. Maki, J. Mahieu, B. C. De. Cooman and S. Claessens: Mater. Sci. Technol. **19** (2003) 125–131.
11) J. Maki, J. Mahieu and B. C. De. Cooman: *Proc. 5th Int. Conf. on Zinc and Zinc Alloy Coated Steel Sheet (Galvatech 2001)*, Bruxelles, Belgium, June 2001, Centre de Researches Meâtallurgiques.
12) P. J. Jacques, E. Girault, A. Mertens, B. Verlinden, J. Van Humbeeck and F. Delannay: ISIJ Int. **41** (2001) 1068–1074.
13) P. J. Jacques, E. Girault, P. Harlet and F. Delannay: ISIJ Int. **41** (2001) 1061–1067.
14) T. K. Han, S. S. Park, K. H. Kim, C. Y. Kang, I. S. Woo and J. B. Lee: ISIJ Int. **45** (2005) 60–65.
15) J. L. Bocos, F. Zubiri, F. Garciandia, J. Pena, A. Cortiella, J. M. Berrueta and F. Zapirain: Weld. Int. **19** (2005) 539–543.
16) S. Daneshpour, S. Riekehr, M. Koçak, V. Ventzke and A.I. Koruk: Sci. Tech. Weld. Join. **12** (2007) 508–515.
17) J. Chen, K. Sand, M. Xia, C. Ophus, R. Mohammadi, M. Kuntz, Y. Zhou and D. Mitlin: Metall. Mater. Trans. A. **39** (2008) 593–603.
18) M. Xia, Z. Tian, L. Zhao and Y. Zhou: Accepted by ISIJ. Int. 2008.
19) S. Morito, H. Tanaka, R. Konishi, T. Furuhara and T. Maki: Acta Mater. **51** (2003) 1789–1799.

20) A. K. De, J. G. Speer and D. K. Matlock: Advanced Materials and Processes: **161** (2003), 27–30.
21) J. O. Andersson, T. Helander and L. H. Hoglund: CALPHAD. **26** (2002) 273–312.
22) S. S. Babu, J. W. Elmer, J. M. Vitek and S. A. David: Acta Mater. **50** (2002) 4763–4781.
23) P. A. Manohar, K. Kunishige, T. Chandra and M. Ferry: Mater. Sci. Technol. **18** (2002) 856–860.
24) S. Kou and Y. Le: Metall. Trans. A. **19** (1988) 1075–1082.
25) D. A. Korzekwa, D. K. Matlock and G. Krauss: Metall. Trans. A. **13** (1982) 2061–2064.
26) L. C. Chang and H. K. D. H. Bhadeshia: J. Mater. Sci. **31** (1996) 2145–2148.
27) C. Garcia-Mateo, F. G. Caballero and H. K. D. H. Bhadesia: ISIJ Int. **43** (2003) 1821–1825.
28) Mertens A. PhD thesis, Universit Catholique de Louvain, Louvain-la-Neuve, Belgium, 2002.
29) N. Rao, V. Bangaru and A. K. Sachdev: Metall. Trans. A. **13** (1982) 1899–1906.
30) S. J. Kim, C. G. Lee, I. Choi and S. Lee: Metall. Mater. Trans. A. **32** (2001) 505–514.
31) I. B. Timokhina, P. D. Hodgson and E. V. Pereloma: Metall. Mater. Trans. A. **35** (2004) 2331–2343.